J. Fluid Mech. (1985), *vol.* 161, *pp.* 269–279
Printed in Great Britain

Measurements of rotating bubble shapes in a low-gravity environment

By FRED LESLIE

Atmospheric Sciences Division, Systems Dynamics Laboratory,
Marshall Space Flight Center, Alabama 35812

(Received 7 March 1985 and in revised form 14 June 1985)

Measurements of rotating equilibrium bubble shapes in the low-gravity environment of a free-falling aircraft are presented. Emphasis is placed on bubbles which intersect the container boundaries. These data are compared with theoretical profiles derived from Laplace's formula and are in good agreement with the measurements. The interface shape depends on the contact angle, the radius of intersection with the container, and the parameter F, which is a measure of the relative importance of centrifugal force to surface tension. For isolated bubbles F has a maximum value of $\frac{1}{2}$. A further increase in F causes the bubble to break contact with the axis of rotation. For large values of F the bubble becomes more cylindrical and the capillary rise occurs over a thinner layer in order that the small radius of curvature can generate a sufficient pressure drop to account for the increased hydrostatic contribution.

1. Introduction

Free-surface shapes of liquids play a key role in spacecraft-fuel-tank design and fluid-management systems. In the absence of gravity and temperature gradients along the surface which drive Maragoni convection, the equilibrium shape of the free surface is governed by a balance of capillary and centrifugal forces. Hydrostatic stability is maintained when the additional pressure from the capillary rise is compensated for by the pressure reduction owing to the curvature of the free surface. In a zero-gravity environment without rotation the surface is spherical. Whether the sphere encloses the liquid or the vapour depends on the wettability of the container by the liquid. In some spacecraft-fuel-tank applications, propellant slosh and distribution are controlled with the use of internal baffles which come into contact with the free surface. If the liquid is to be held using capillary forces, the baffle spacing must be small enough to overcome the fluid's inertial forces during small accelerations brought about by thruster firings, crew motion, etc. The problem can be complicated by the rotation of the container. In any case, in order to manage the liquid the distribution of the fluid including its interface shape must be determined.

Rosenthal (1962) computed the shapes of rotating bubbles in the absence of gravity. He found that for large rotation rates the aspect ratio of a free bubble is proportional to the square of the rotation rate. Chandrasekhar (1965) examined the stability of a rotating liquid drop and derived analytical formulas for the equilibrium shapes based on Laplace's equation for the pressure drop across the interface. He went on to determine the frequency of the oscillations for various modes. Busse (1984) also examined the frequency of small oscillations for drops and bubbles. Using a spherical coordinate system he determined the equilibrium shape for a rotating liquid drop in terms of a Legendre-function expansion. He determined that, for drops, the frequency

of oscillation increases with rotation rate. The opposite result occurs for bubbles. Tieu, Joseph & Beavers (1984) obtained solutions for the motion and interface shape of a two-fluid system contained in an oscillating vertical cylinder. Using a domain perturbation approach, they obtained first- and second-order solutions in a standard-gravity environment. Experimental results were in qualitative agreement with their theoretical predictions.

Princen, Zia & Mason (1967) measured interface-shape characteristics of bubbles. However, in order to perform the experiments in a standard-gravity environment, the rotation rate had to be high enough for centrifugal forces to be much greater than gravitational forces. Consequently, the bubble interfaces were shaped like cylinders with round ends. Gans (1985) obtained numerical solutions for rotating bubbles enclosed in baffled containers and found that gravity had a destabilizing influence on their position. The solutions were validated experimentally in a standard-gravity environment. Experiments with non-axisymmetric shapes of a rotating drop immersed in a host medium were performed by Wang *et al.* (1982). They observed a family of multilobe shapes as a function of a rotational bond number. Experimental results have also been obtained by acoustic excitation of drops (Trinh, Zwern & Wang 1982).

In this paper measurements of rotating equilibrium free-surface shapes in the low-gravity environment of a free-falling aircraft are presented. This allows variation of the relative importance of surface tension with respect to centrifugal forces, producing a variety of shapes for comparison with theoretical profiles. Calculations of the shapes are made using a more general formulation of Chandrasekhar's equation by including contact of the interface with the rotating container at a specified angle. It is easily shown that an isolated bubble or drop is a special case of the general result. Section 2 describes the experimental apparatus used to generate the rotating liquid surfaces as well as the low-gravity environment produced by the aircraft. The data-reduction technique is also discussed. The analytical derivation of the model is presented in §3 along with the regime of solutions. Finally, §4 contains a comparison of the two results and discussion.

2. Experimental technique

A schematic of the apparatus is shown in figure 1. It consists of a Plexiglas cylinder 20 cm in diameter, the depth of which can be set at 2, 4 or 6.3 cm. The cylinder is partially filled with ethanol, chosen because: its surface tension is relatively high and not extremely sensitive to low levels of contamination; its contact line with the container does not stick; and its contact angle is close to zero. The cylinder is fastened to a turntable which rotates about the cylinder's axis. The rotation speed can be varied from 0 to 108 rev./min. After the cylinder is filled with ethanol, a prescribed amount is removed to establish the bubble volume. Overhead and side-mounted video and still cameras record the shape of the fluid interface.

The apparatus was bolted to the floor of a KC-135 aircraft, which is flown in a parabolic trajectory that provides 20–30 s of low gravity. Figure 2 shows a typical trajectory. After a descent from about 35000 ft to 25000 ft the aircraft attains an airspeed of 520 m.p.h. and then pitches sharply upward to begin the parabola. The local gravity environment begins to diminish to near zero and is measured by accelerometers. Although the gravity fluctuates around zero, typical departures are no more than 2% of terrestrial gravity. At the top of the arc, near 35000 ft, the airspeed has reduced to 320 m.p.h. and the aircraft pitches down for the second half

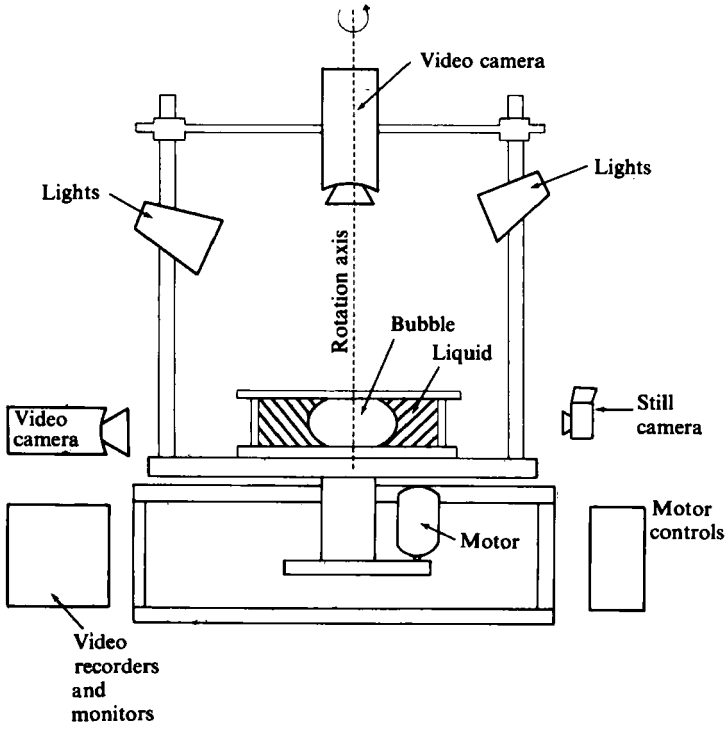

FIGURE 1. A schematic of the experimental apparatus.

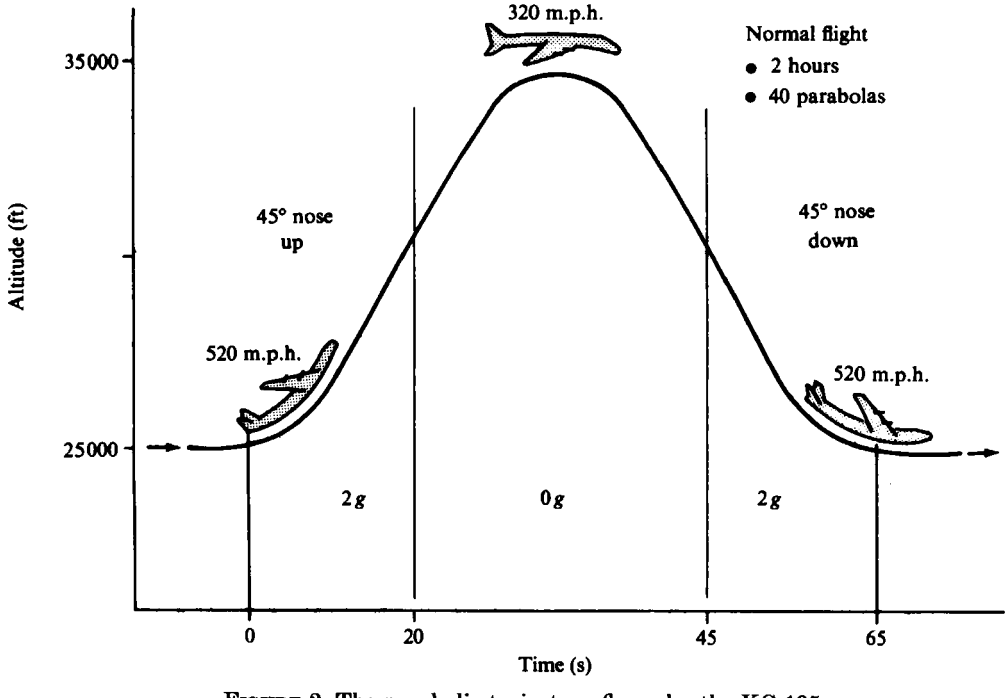

FIGURE 2. The parabolic trajectory flown by the KC-135 aircraft for the low-gravity manoeuvre.

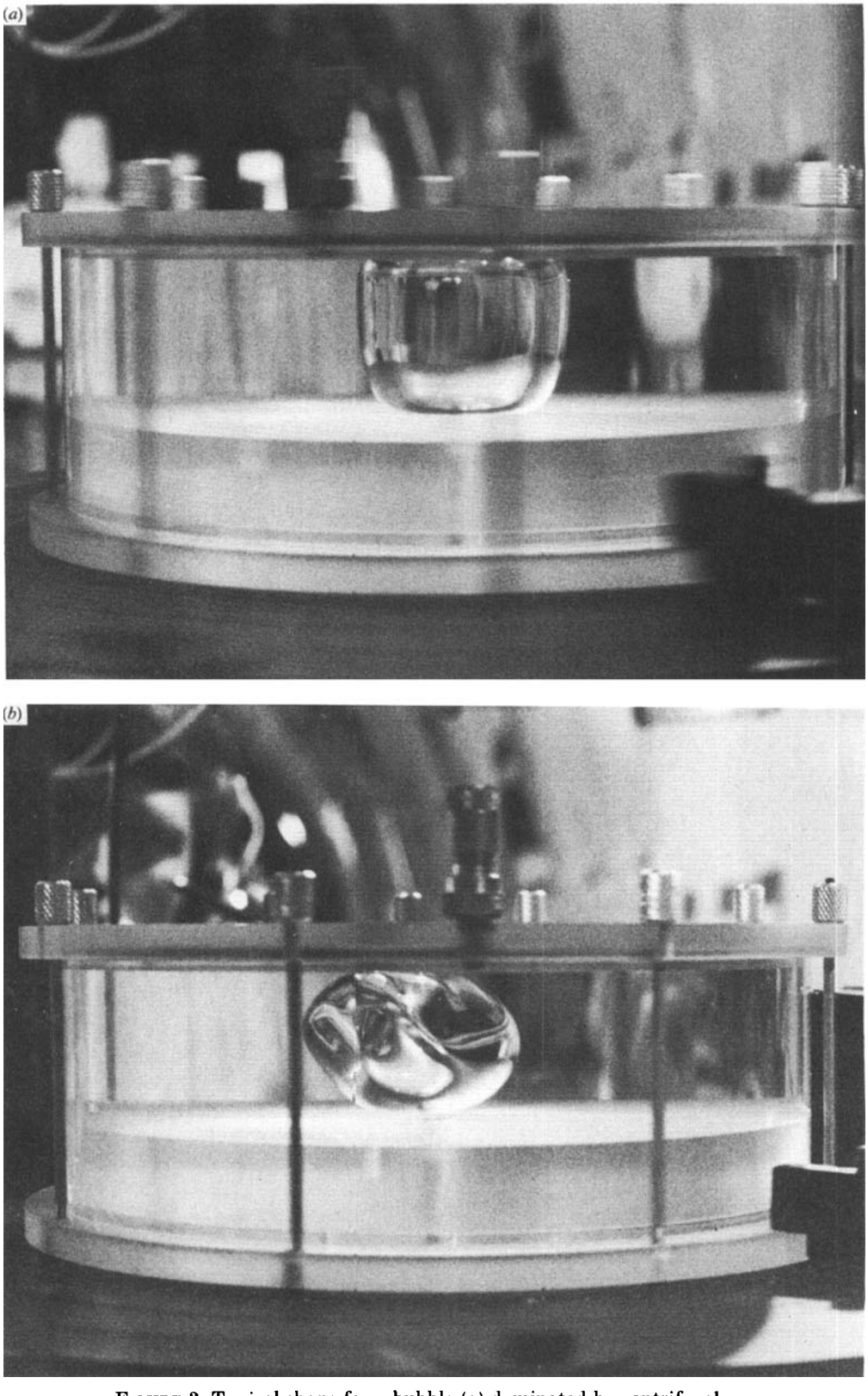

FIGURE 3. Typical shape for a bubble (*a*) dominated by centrifugal force and (*b*) dominated by surface tension.

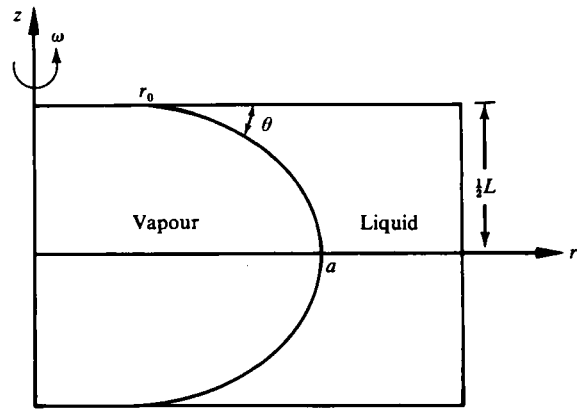

FIGURE 4. Definition sketch for the cylindrical coordinate systems used for the analytical model.

of the parabola. The manoeuvre is completed when the aircraft has descended to 25000 ft and another parabola begins.

The fluid is set into rotation before the manoeuvre begins and the bubble shape is determined primarily by the centrifugal and gravitational forces, producing the classic paraboloidal surface. During the aircraft pullout at the start of the manoeuvre, the fluid experiences a force of 2 g which tends to flatten the bubble at the top of the cylinder. As the local gravity diminishes the vapour penetrates down the axis of the cylinder. The interface appears as a meniscus symmetric about the axis. Figure 3 shows typical bubbles for (*a*) rotation relatively strong compared to surface tension, and (*b*) weak rotation. For the latter case, the bubbles tend to meander somewhat and their shape is more sensitive to fluctuations of the low-gravity environment. This is consistent with Rosenthal's analytical result that rotation has a stabilizing effect.

Analysis of the data is performed in four steps. First, a photographic frame of the bubble is digitized to provide coordinates for the liquid–vapour interface. Next, the shape is scaled to actual size using ratios of known dimensions. Then, the data is corrected for optical distortion using a ray-trace algorithm. Finally, the volume of the bubble is computed from the coordinates of the interface and compared with the measured value.

3. Analytical model

Chandrasekhar's (1965) analysis is expanded to develop an equation for the interface shape relevant to the present application. Figure 4 shows the cylindrical coordinate system used for the derivation. The bubble is assumed to be symmetric about the axis as well as its equator. The latter is valid for a zero-gravity environment and simplifies the derivation. The fluid interface intersects the top of the cylinder at a height L and at a radius r_0 and makes an angle θ. The bubble has a radius a. The pressure inside the bubble p^{i} is given by

$$p^{\mathrm{i}} = p_0^{\mathrm{i}} + \tfrac{1}{2}\rho^{\mathrm{i}}\omega^2 r^2, \tag{1}$$

where p_0^{i} is a constant, ρ^{i} is the density of the fluid inside the interface and ω is the rotation rate of the fluid. The pressure outside the bubble p^{o} is given by

$$p^{\mathrm{o}} = p_0^{\mathrm{o}} + \tfrac{1}{2}\rho^{\mathrm{o}}\omega^2 r^2, \tag{2}$$

where p_0^o is a constant, and ρ^o is the density of the fluid outside the interface. At the interface, the pressure discontinuity is given by Laplace's formula

$$p^i - p^o = T\nabla\cdot\hat{\boldsymbol{n}}_0, \tag{3}$$

where T is the coefficient of surface tension and $\hat{\boldsymbol{n}}_0$ is the unit normal pointing outward from the surface. Let the position of the interface be given by $z = f(r)$. Then the right-hand side of (3) is

$$-T\frac{\mathrm{d}}{\mathrm{d}r}\frac{r\phi}{(1+\phi^2)^{\frac{1}{2}}},$$

where $\phi \equiv \mathrm{d}f/\mathrm{d}r$. Substituting (1) and (2) into (3) yields

$$p_0 r + \tfrac{1}{2}\rho\omega^2 r^2 = -T\frac{\mathrm{d}}{\mathrm{d}r}\frac{r\phi}{(1+\phi^2)^{\frac{1}{2}}}, \tag{4}$$

where $p_0 \equiv p_0^i - p_0^o$ and $\rho \equiv \rho^i - \rho^o$. One integration of (4) results in

$$\tfrac{1}{2}p_0 r^2 + \tfrac{1}{8}\rho\omega^2 r^4 = -\frac{Tr\phi}{(1+\phi^2)^{\frac{1}{2}}} + C,$$

where C is a constant. The value of C can be determined by the boundary condition that, at $r = r_0$, $\phi = -\tan\theta$. The value of p_0 can be evaluated at $r = 0$ where $\phi \to -\infty$. With these substitutions and non-dimensionalizing r and z with a, the general equation for the interface becomes

$$f(\hat{r}) = \int_1^{\hat{r}} \frac{\psi}{(1-\psi^2)^{\frac{1}{2}}}\,\mathrm{d}\hat{r}, \tag{5}$$

where

$$\psi = \frac{1-\hat{r}_0\sin\theta + F(1-\hat{r}_0^4)}{1-\hat{r}_0^2}\frac{\hat{r}_0^2-\hat{r}^2}{\hat{r}} + \frac{F(\hat{r}^4-\hat{r}_0^4)}{\hat{r}} - \frac{\hat{r}_0\sin\theta}{\hat{r}},$$

and $(\hat{})$ denotes non-dimensional radii, while F is a parameter defined as $F \equiv (\rho^o - \rho^i)\omega^2 a^3/T$. It represents the ratio of centrifugal force to surface tension. F is negative for rotating drops ($\rho^i > \rho^o$) and positive for rotating bubbles ($\rho^i < \rho^o$). Note, if $\hat{r}_0 = 0$ and $\theta = 0$, (5) is equivalent to Chandrasekhar's equation for the shape of a rotating free drop. Also for the additional case of $F = 0$, (5) represents a sphere.

Chandrasekhar presented solutions for drops in which $\hat{r}_0 = 0$, $\theta = 0$, and F is negative. He showed that the boundary conditions for the equations could be met only for $F > -2.32911$. Otherwise, the rotation was strong enough to centrifuge all the liquid away from the axis, forming a torus-like drop.

This investigation examines rotating bubbles which may intersect the top and bottom boundaries. In this case $F > 0$ and $\hat{r}_0$ may not be 0. It can be shown that there is a maximum value of F above which the bubble interface no longer contacts the axis. By taking the derivative of ψ with respect to $\hat{r}$ and setting it equal to zero, we can see that ψ is a maximum at $\hat{r} = [(1+F)/3F]^{\frac{1}{2}}$. Setting this maximum equal to 1 and solving for F gives $F = \frac{1}{2}$. Considering the denominator of (5), it is clear that, in general, solutions exist only for $\psi^2 < 1$. This places a constraint on the relation between F and $\hat{r}_0$. Figure 5 shows plots of the solution regimes for various contact angles. It can be seen that as the centrifugal force increases and F becomes more positive the radius of intersection with the boundary increases. Physically, the fluid is being centrifuged away from the axis and the fluid intersects the boundary at a larger radius. As the rotation increases without limit the vapour core approaches in

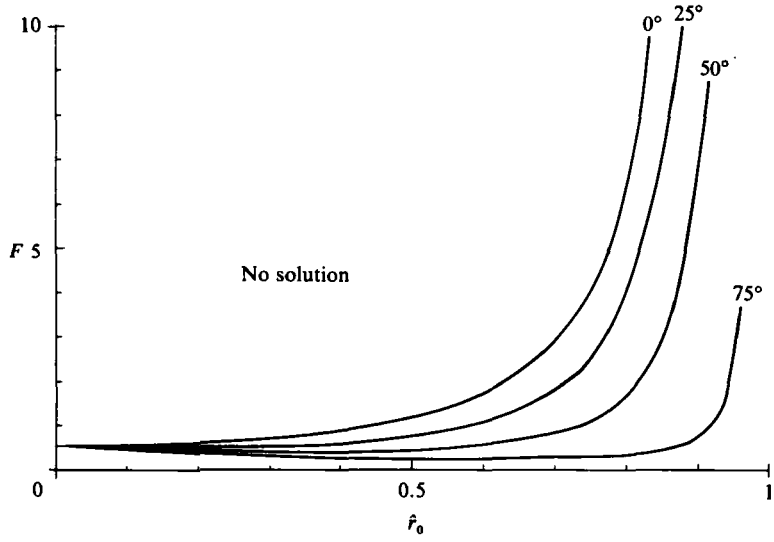

FIGURE 5. Solution regime of (5) for various contact angles.

shape a cylinder whose radius is governed by the vapour volume and L. The radius of intersection is particularly sensitive to F until F exceeds about one. Thus when centrifugal forces dominate, the interface becomes more nearly parallel with the rotation axis except at the boundaries, where it must satisfy the contact-angle constraint. As the contact angle increases, the intersection radius naturally increases. To summarize, for an isolated bubble ($\hat{r} = 0$ and $\theta = 0$), the shape of the bubble is determined solely by the parameter F. This parameter ranges from 0 for a spherical bubble to $\frac{1}{2}$ for a cylindrical bubble. From the definition of F it can be seen that, for a constant F, a further increase in the rotation speed reduces the bubble radius, which increases its length to conserve volume. Values of F greater than $\frac{1}{2}$ can be permitted only if the top of the bubble breaks contact with the axis. Then permissible values of F are determined by the contact radius of the interface with the boundary.

4. Discussion of results

Measurements of free-surface shapes were compared with the model calculations for various values of F, $\hat{r}_0$ and L. For the calculations, the values of F and L as well as the vapour volumes were known from the experiment. The value of F was entered into (5). The value of r_0 could not be easily determined from the overhead or side cameras, particularly since θ is near zero. Instead, a guess of $\hat{r}_0$ was made and the equation was numerically integrated. If the computed value of z at $\hat{r} = \hat{r}_0$ was not equal to the known cylinder half-depth, a new guess for $\hat{r}_0$ was made. After the integration was complete, a check of the measured bubble volume with the computed volume was made.

Figure 6(*a–c*) shows a comparison of the measured interface profiles with the calculated ones for small, moderate, and large values of F respectively. The cylinder depth is 2 cm. The profile in figure 6(*a*) is a low-rotation case which is dominated by capillary forces. These data were somewhat difficult to obtain because the equilibrium was very sensitive to the environment's departure from zero gravity. Although the fluid quickly transitioned to a quasi-steady state as the environmental

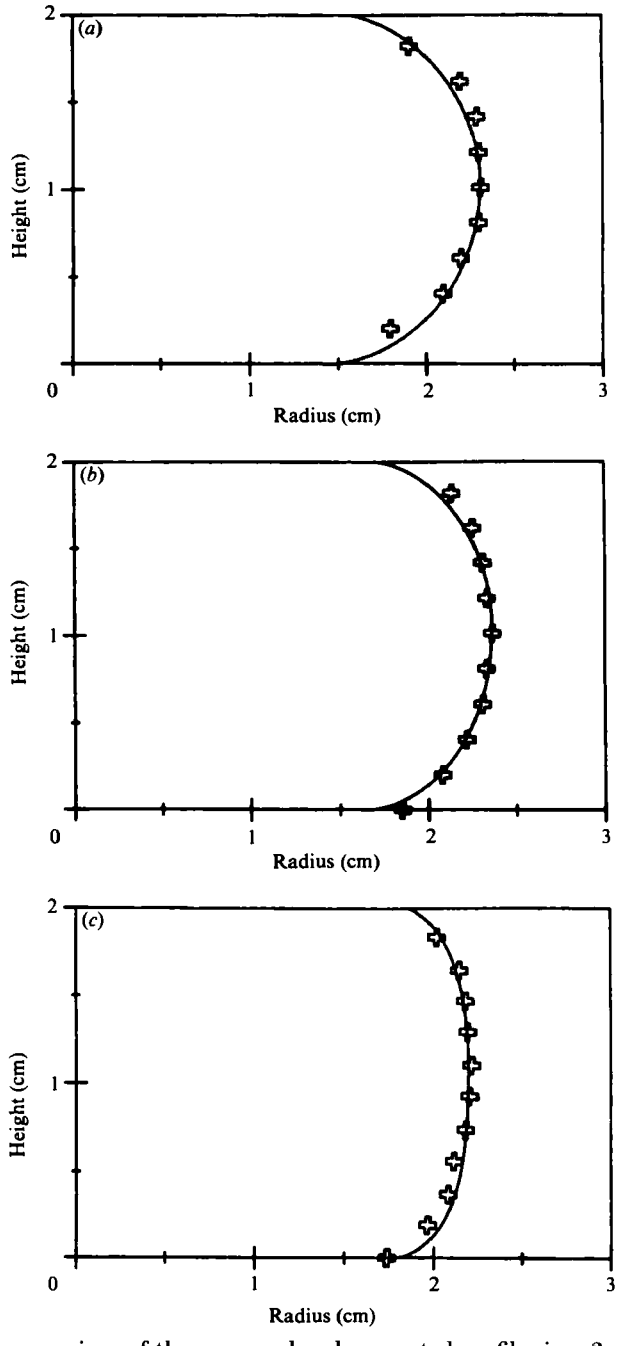

FIGURE 6. A comparison of the measured and computed profiles in a 2 cm deep cylinder for (*a*) $F = 0.16$, (*b*) 1.1, and (*c*) 5.6. ✣ , measurement; ——, equation (5).

gravity diminished from 2 g to near zero, establishment of a true equilibrium was transitory. Fluctuations around zero gravity created vertical displacements of the bubble which sometimes broke contact with the top or bottom boundaries. Clearly for this case the interface surface is near spherical and is in good agreement with the calculations.

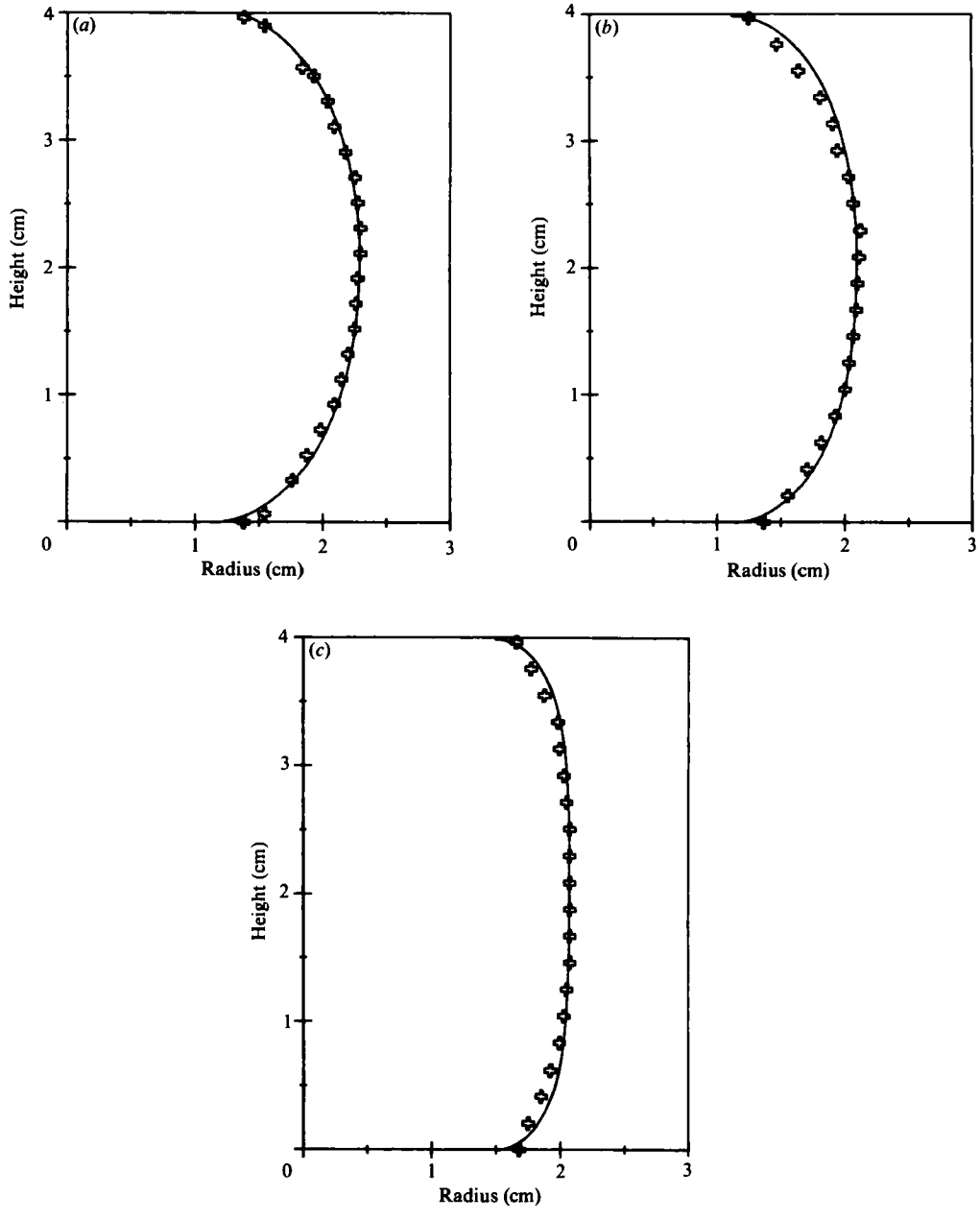

FIGURE 7. A comparison of the measured and computed profiles in a 4 cm deep cylinder for (*a*) $F = 0.71$, (*b*) 0.99, and (*c*) 3.2. ✥, measurement; ——, equation (5).

Figure 6 (*b*) shows data for a moderate value of F. Here the capillary and centrifugal forces are about equal and the surface has become more prolate. It can be seen that the value of $\hat{r}_0$ has increased, consistently with figure 5. Similarly, figure 6 (*c*) shows the data and calculated profiles for a large value of F. The surface here is dominated by centrifugal force and the interface is more parallel with the rotation axis, except at the boundary, where it is constrained to intersect at a prescribed angle. For this

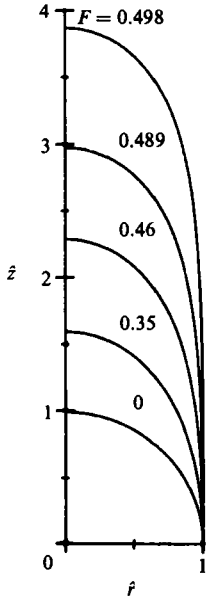

FIGURE 8

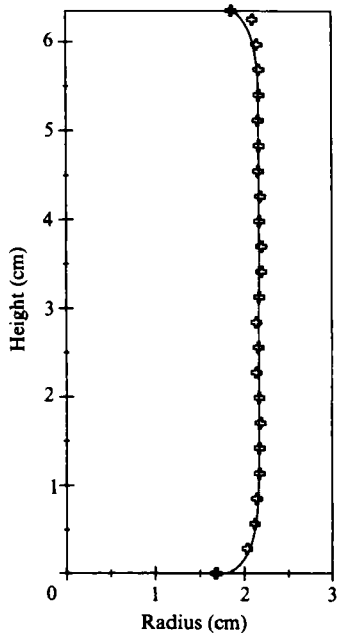

FIGURE 9

FIGURE 8. Computed interface shapes for isolated bubbles for various values of F.

FIGURE 9. A comparison of the measured and computed profiles in a 6.3 cm deep cylinder for $F = 6.4$. ✣, measurement: ——, equation (5).

value of F the interface was quite stable because the centrifugal force was not only greater than the capillary force, but was also much greater than the fluctuating residual environmental gravity.

Figure 7 (a–c) shows interface shapes for a cylinder depth of 4 cm. For a given bubble volume larger rotation rates are needed in order for the bubble to contact the top and bottom boundaries as required by the theory. Otherwise, the bubble with a smaller diameter than the cylinder gap meanders along the axis or attaches to the top or bottom boundary. Figure 7 (a) represents one of the slower relative rotation rates that could stabilize the bubble. Equation (5) can be used to determine the largest gap required to stabilize a bubble at a particular value of F. The tallest bubble that can be attained for a given F is found by using the smallest $\hat{r}_0$ that the solution will permit. Figure 8 shows computations of the interface shapes of isolated bubbles ($\hat{r}_0 = 0$) for various values of F. It is apparent that increasing the rotation increases the aspect ratio of the bubble. This occurs as F approaches its maximum value of $\frac{1}{2}$ for an isolated bubble. A further increase in F after that point causes the bubble to break contact with the axis of rotation and $\hat{r}_0$ becomes greater than 0. Once $\hat{r}_0$ increases then the solution permits larger values of F consistent with figure 5. Figure 7 (b) shows a profile in which centrifugal and capillary forces are about equal. The value of F is about the same as for the profile in figure 6 (b). However, $\hat{r}_0$ had to be appropriately decreased for the computation in order for the interface height to match the deeper container. Figure 7 (c) shows an interface profile for $F = 3$. Because capillary forces are weak, the interface is almost cylindrical except for its contact point with the top and bottom boundaries. The capillary rise occurs over a

thinner layer in order that the small radius of curvature can generate a sufficient pressure drop to account for the increased hydrostatic contribution.

Finally, figure 9 shows an interface profile for a rotating cylinder of 6.3 cm depth. For similar bubble-volume to total-volume ratios, higher values of F are required to produce an interface with top and bottom boundary contact. This simply means that they require greater rotational speeds, since for these near-cylindrical bubbles the bubble radius changes little with ω. An increase in ω merely increases F, producing a more nearly cylindrical bubble. The figure shows the resulting thinner layer over which the surface tension acts to meet the contact-angle requirement. This layer is thinner for the reason stated above.

In summary, (5) derived from Laplace's equation relating the pressure drop across an interface to the radii of curvature has been applied to a rotating bubble which contacts the container boundary. Solutions to the equation are dependent upon several parameters, namely F the ratio of centrifugal to capillary forces, $\hat{r}_0$ the contact radius of the interface to the boundary, and also θ the contact angle. For the cases presented here the contact angle was near zero, which permits a greater range of solutions. For isolated bubbles F has a maximum value of $\frac{1}{2}$. A further increase in F causes the bubble to break contact with the axis of rotation. For larger values of F, the bubble becomes more cylindrical and the capillary rise occurs over a thinner layer. Measurements of the interface shapes performed in the low-gravity environment of an aircraft following a parabolic trajectory showed good agreement in the cases examined.

The author wishes to acknowledge the efforts of Roger Gans and Charles Schafer who provided assistance with the experimental aspects of this work. The author would also like to thank Robert Shurney for his help in coordinating the aircraft activities. This work was supported by the Marshall Space Flight Center Discretionary Fund no. 83-21.

REFERENCES

Busse, F. H. 1984 Oscillations of a rotating liquid drop. *J. Fluid Mech.* **142**, 1.

Chandrasekhar, F. R. S. 1965 The stability of a rotating liquid drop. *Proc. R. Soc. Lond.* A **286**, 1.

Gans, R. F. 1985 Liquid management in low gravity using baffled containers. *AIAA J. Spacecraft and Rockets.* **22**, 287.

Princen, H. M., Zia, I. Y. Z. & Mason, S. G. 1967 Measurement of interfacial tension from the shape of a rotating drop. *J. Colloid Interface Sci.* **23**, 99.

Rosenthal, D. K. 1962 The shape and stability of a bubble at the axis of a rotating liquid. *J. Fluid Mech.* **12**, 358.

Tieu, H. A., Joseph, D. D. & Beavers, G. S. 1984 Interfacial shapes between two superimposed rotating simple fluids. *J. Fluid Mech.* **145**, 11.

Trinh, E., Zwern, A. & Wang, T. G. 1982 An experimental study of small-amplitude drop oscillations in immiscible liquid systems. *J. Fluid Mech.* **115**, 453.

Wang, T. G., Tagg, R., Cammack, L. & Croonquist, A. 1982 Non-axisymmetric shapes of a rotating drop in an immiscible system. In *Proc. 2nd Intl Colloquium Drops and Bubbles*, vol. 82–7, p. 203. JPL.